PII: S0955-2219(98)00156-3

0955-2219/98/$—see front matter

Biomorphic Cellular Silicon Carbide Ceramics from Wood: I. Processing and Microstructure

Peter Greil,* Thomas Lifka and Annette Kaindl

University of Erlangen-Nuernberg, Department of Materials Science, Glass and Ceramics, Martensstr. 5, D-91058 Erlangen, Germany

(Received 20 March 1998; revised version received 10 June 1998; accepted 16 June 1998)

Abstract

Processing of cellular ceramics with anisotropic pore structures by infiltration of liquid Silicon into carbonized wood and subsequent reaction to SiC was investigated. Natural wood of different pore size distribution and composition was carbonized at 800–1800°C in inert atmosphere resulting in a one-to-one reproduction of the original wood structure. The carbon template was converted to SiC by a rapid liquid infiltration-reaction process at 1600°C. Spontaneous infiltration was achieved by using the continous tracheidal cells in wood as a transportation path for liquid silicon. β-SiC formed by solid–liquid reaction at the pore surface exhibits a crystalline texture which may be related to the initial microfibril orientation in the cell walls of wood. Depending on the initial cellular microstructure of the various kinds of wood (ebony, beech, oak, maple, pine, balsa) ceramic materials of different anisotropic pore structures in the form of pseudomorphs of the original wood were obtained.

1 Introduction

Material synthesis from biological structures has recently attained particular interest.[1–4] Due to the genetic evolution process, biological structures exhibit excellent strength at low density, high stiffness and elasticity, and damage tolerance on a micro as well as on a macro scale. Particular research effects have been devoted to biomineralization processes where precipitation of inorganic phases such as phosphates, carbonates, sulfates, etc. is stereochemically controlled by a moving organic-inorganic phase boundary (biomembrane).[5–9] Due to the low temperatures from room temperature to 100°C, however, growth rates are usually very slow (μm/h^{-1}) so that bulk ceramic materials could not be processed in reasonable processing time yet.

A significant, increase of synthesis rates can be achieved when cellular biological structures with an open porosity system accessible to liquid or gaseous infiltrants are used for high temperature reaction processes. Natural fibers such as sisal, jute, hamp, etc. were infiltrated with $AlCl_3$, and $TiCl_4$, respectively, and subsequently transformed to oxidic Al_2O_3, and TiO_2, fibers by annealing in air.[10,11] Cotton fibers coated with Si_3N_4 were converted to SiC fibers by annealing in Ar-atmosphere at 1200–1600°C.[12] Recent activities are directed to the question how to transform the hierarchical cellular structure of wood into inorganic materials with specific functional properties. Wood is a natural composite with cellulose, hemicellulose, and lignin as the major biopolymeric constituents and additional macromolecular compounds like different kinds of fat, oil, wax, resin, sugar, minerals, alcaloides, etc. as minor constituents. The average elemental composition of wood is 50 wt% C, 43·4 wt% O, 6·1 wt% H, 0·2% N and 0·3 wt% ash.[13] A typical composition of softwood is 48 wt% cellulose, 19 wt% hemicellulose and 30×wt% lignin which differs only slightly from hardwood which is 45, 27 and 22 wt%, respectively.[13] The molecular structures and compositions of the major biopolymers hemicellulose, cellulose and lignin are very complex and may vary for different kinds of wood. The polysaccharide cellulose is of particular significance for the microscopic cell wall structure, which is a natural fiber reinforced composite of cellulose fibers (macrofibrils) embedded in a matrix of hemicellulose and lignin. The fiber orientation in the cell wall exerts a strong

*To whom correspondence should be addressed.

influence on the shrinkage behavior of wood and the mechanical properties.[14] The cells forming natural wood can be roughly distinguished with respect to their function into tracheidal (transportation), parenchymal (storage) and libriformal (mechanical strengthening) cells.[13] Mesoscopically, the tracheidal cells (vessels) of hardwood which may attain a length of μm up to several m, can be arranged into rings (ring porous anatomy or be evenly distributed over the cross section of wood perpendicular to the growth direction (diffusive porous anatomy). While oak is of ring porous anatomy, maple, beech, balsa and ebony are diffusive porous wood. respectively, Macroscopically, wood is characterized by formation of growth ring structures which are the reason for the macroscopic inhomogeneity of natural wood. The microstructural features of wood range from mm (growth ring strictures) via μm (tracheidal cell palterns, macro- and microfibril cell wall textures) down to nm scale (molecular fiber and membrane structures of cell walls), (Fig. 1). Due to this unique hierarchical architecture of the cellular microstructure wood exhibits a remarkable combination of high strength, stiffness and toughness at low density.[14,15] The properties, however, strongly depend on the loading direction with respect to the cell orientation (e.g. axial, radial and tangential) making wood to an example of an extremely anisotropic material.

Heating wood in non-oxidizing atmosphere at temperatures above 600°C results in decomposition of the polyaromatic constitutents to form a carbon residue which reproduces the originial cellular structure. SiC with highly anisotropic porosity was produced from wood by liquid infiltration of the carbonized preform with tetraethylorthosilicate (TEOS) and subsequent heating to 1400°C in Ar.[16] The carbon structure may also serve as a template for a variety of alternative reaction processes.[17] The development of novel wood derived ceramics, however, requires to control the transformation of the hierarchical microstructural features of wood at all hierarchical levels into an equivalent microstructure of the inorganic reaction product. In part I of this work, results on the use of various wood materials as microstructural templates for producing hierarchically structured SiC-ceramic materials by liquid Si infiltration and reaction process (LSIR) will be discussed. The mechanical behavior of the resulting cellular SiC/(Si)-materials was examined with respect to the anisotropic arrangement of the pore channel system and will be presented in part II of this work.

2 Experimental Procedure

Different kinds of natural wood were used to produce SiC-ceramics with different fractional densities and porosity structures, Table 1. The inital porosities ranged from 32% for ebony to 55–67% for beech, oak, maple and pine up to >90% for balsa, respectively. Maximum diameters for the tracheidal cells were in the range of 50 μm for pine up to 350 μm for oak. Rectangular specimens ($10\times10\times60\,mm^3$) of the carbon preform were prepared by pyrolyzing the dried (70°C, 15 h) wood in N_2-atmosphere in a carbon heated furnace. A slow heating rate of $1°C\,min^{-1}$ was applied up to 500°C where the polyaromatic hydrocarbon polymers (cellulose, hemicellulose, lignin) have completely decomposed to carbon followed by a higher rate of $5°C\,min^{-1}$ up to the peak temperature. The specimens were held at a temperature in the range from 800–1800°C for 4 h. The porous carbon preform was infiltrated with liquid silicon in carbon dies at 1600°C without pressure according to the conventional processing of SiSiC-materials.[18–20] Spontaneous infiltration could be achieved for

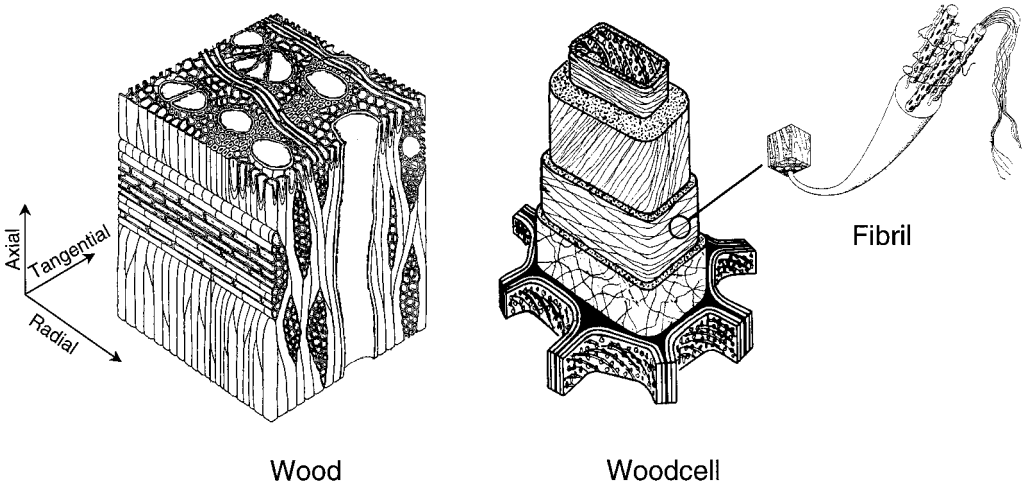

Fig. 1. Hierarchical microstructure of wood. (a) macroscopic and (b) microscopic cell structure.

Table 1. Characteristics of wood[13]

	Oak Quercus robus	*Maple* Acer pseudoplatanus *L*	*Beech* fagus silvatica *L*	*Ebony* Diosppyros celebica *Bakh*	*Balsa* Ochroma lagopus *SW*	*Pine* pinus silvestris *L*
Composition						
Celullose (wt%)	38–43	38	34–46	44	50–54	42–52
Pentosane (wt%)	19–26	20	18–25	17	18–19	8–13
Lignin (wt%)	25–34	25	12–23	48	22–27	26–31
Structure						
Tracheas (vol%)	sp 39, lp 8	7	40	10	3–4.5	93
Parcrichyms (vol%)	5	—	5	13	74	
Libriforms (vol%)	44	76	40	57	4	
Trach. diameter (μm)	ew 150–350 lw 0–140	30–70	8–85	70–115	130–200	ew 18–54 lw 12–25
Porosity	57	61	55	32	91	67
Density (g/cm^3)	0.39–0.93	0.48–0.75	0.68–0.880.9	1.03	0.05–0.13	0.49–0.86
Shrinkage						
axial (%)	0.4	0.5	0.3		0.6	0.2–0.4
radial	4.0–4.6	3	5.8	8.2	1.8–3.0	3.3–4.5
tangential	7.8–10	8	11.8	12.8	3.5–5.3	7.5–8.7
Strength						
bending (MPa)	74–105	50–140	74–210	100–120	1.9–5.3	41–205
compression	54–67	29–72	41–99	60–70	2.7–9.4	35–94
tension axial	50–180	82–114	57	180	7.5	35–196
tension rad., tang.	2.6–9.6			2.2–3.8	1	1–4.4
Youngs Modulus						
axial (GPa)	10–13.2	6.4–15.2	10–18	10	11–6	6.9–20.1
radial, tangential					0.6–1.2	2.7–11.2

(sp: small pores; lp: large pores; ew: early wood, lw: late wood).

different specimen orientations e.g. axial, radial and tangential access of silicon melt. The specimens were kept for 4 h at this temperature to allow complete reaction of silicon with the carbon structure to form β-SiC. Unreacted silicon remained in part of the pore channels so that a celullar Si-containing SiC composite material finally was obtained. Figure 2 summarizes the processing scheme.

While the organic/inorganic transformation of natural wood is strongly affected not only by the molecular constituents e.g. cellulose and lignin but also by the cellular pore channel system specimens of the isolated biopolymers may give more detailed information on the role of molecular chemistry for carbonization process. Thus, for comparison powders of cellulose (Lot No 9004-34-6) (typical composition in wt%: C 44·4, O 49·4, H 6·2) and lignin (Lot No 8072-93-3) (typical composition in wt% C 63·2, O 30·7, H 6·1) (Sigma Aldrich Chemie, Steinheim, Germany) were treated under the same conditions as the wood samples in order to examine the effect of molecular structure of the biopolymer precursor on the carbon microstructure generation. The conversion from the bioorganic to the inorganic ceramic material was monitored by thermal balance analysis (STA 409, Netzsch Gerätebau, Selb, Germany). Density and porosity were measured by Helium pycnometry (Accu Pyk 1330, Micromeritics, Düsseldorf, Germany). Distribution of tracheidal

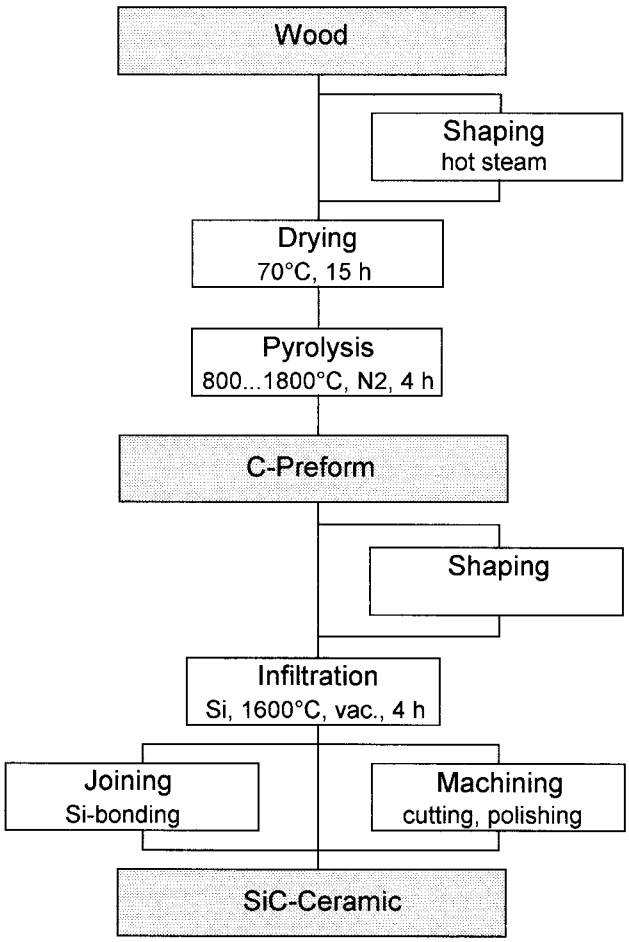

Fig. 2. Processing scheme of manufacturing cellular β-SiC ceramics from wood.

cell diameters was determined by stereological analysis of SEM micrographs of axial cross sections. The microstructures of the intermediate and final products were characterized by SEM (Stereoscan S 2150 MK3, Cambridge Instruments. Cambridge, UK). The degree of crystallinity of the pyrolyzed carbon was determined from the (0002) peak of hexagonal carbon by XRD (D 500, Siemens, Karlsruhe, Germany) according to the method given by Ref. 21. Monochromated CuKα radiation was used. The molecular microstructure of the pyrolyzed carbon preform was examined by high resolution TEM with 300 kV (CM 300 ultratwin, Philips, Eindhoven, The Netherlands) which attains a point resolution of 0·18 nm. Electron backscattered analysis (EBSD) with 20 kV (Link Oxford, Oxford, GB) was used to identify preferential orientations of β-SiC formed by the solid–liquid reaction of silicon with the carbon preform. Residual silicon content after infiltration and reaction was determined by wet chemical analysis. Powdered samples were etched in an aqueous solution of HF/HNO_3, at room temperature to dissolve elemental silicon present in the open tracheidal

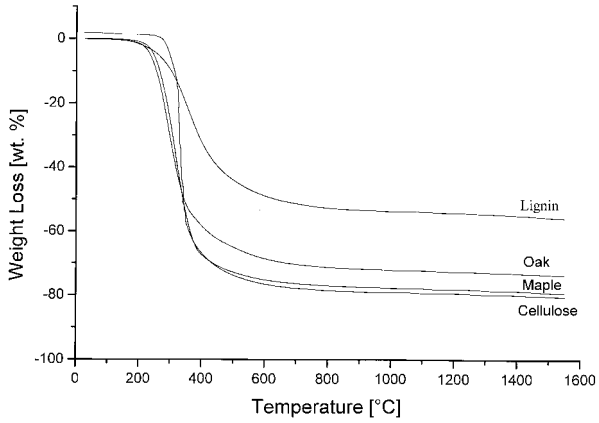

Fig. 3. Weight loss during heating of wood-powder in inert atmosphere.

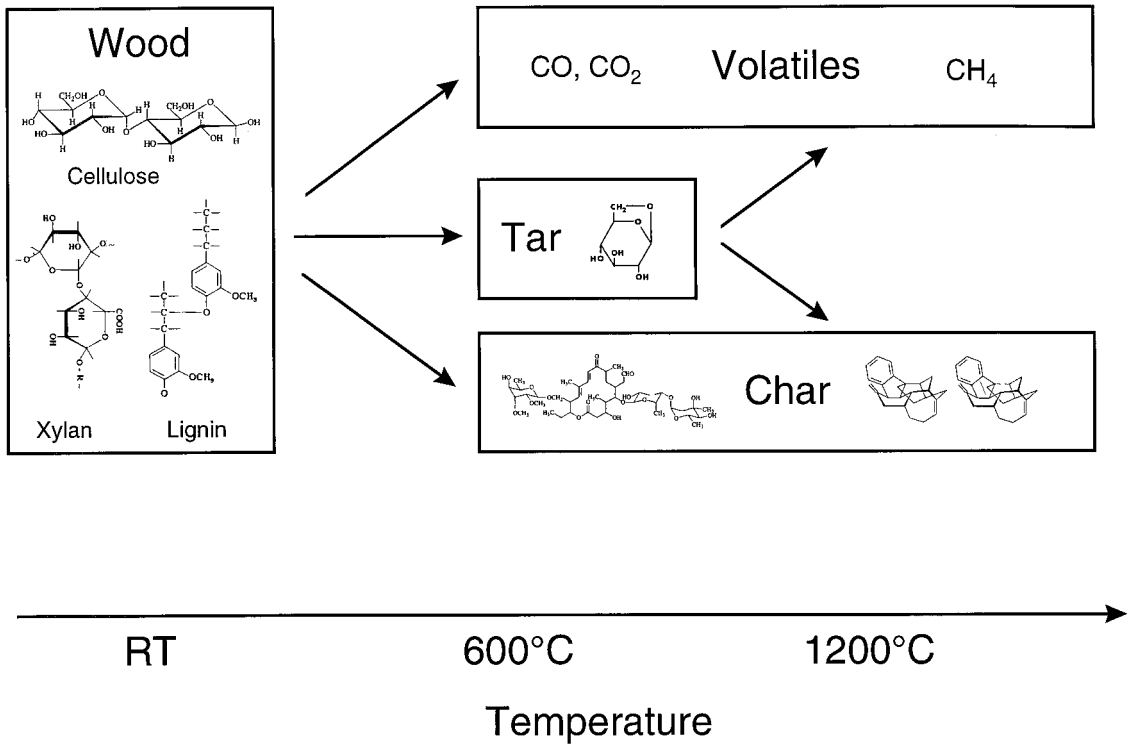

Fig. 4. Thermal decomposition products of the major molecular constituents of wood.

Table 2. Microstructural characteristics of wood after pyrolysis at 1800°C and subsequent Si-infiltration at 1600°C

Wood		*Balsa*	*Pine*	*Oak*	*Maple*	*Beech*	*Ebony*
Pyrolysis weight loss (wt%)		73·5	73·8	70·4	74·9	74·2	64·6
Pyrolysis	axial	21	23	17	20	22	14
shrinkage (%)	radial	22	28	28	30	32	25
	tangential	22	31	33	40	38	30
Density (g cm^{-3})	pyrolyzed	0·06	0·31	0·50	0·51	0·55	0·87
	Si-infiltrated	2·02	2·22	2·16	2·58	2·57	—
Porosity (%)	Pyrolyzed	22/70	21/57	30/40	43/22	42/21	23/20
(open/closed)	Si-infiltrated	11/14	11/14	8/5	3/5	3/2	3/-
Si-content (wt%)		67	50	27	23	37	—

pore channels. Si-content in the solution was measured by ICP (Spectroflame, Spectro Analytical Instr., Kleve, Germany).

3 Results

3.1 Pyrolytic conversion of wood to carbon preform

Weight loss during heating of dried wood in inert atmosphere starts below 200°C and is almost terminated at 500–600°C, (Fig. 3). Various maxima in decomposition rate at approximately 280, 340 and 400°C, respectively, could be detected which are associated with the pyrolytic decomposition of hemicelluclose, cellulose and lignin.[22] While the theoretical carbon content of wood is approximately 50 wt% significantly higher weight losses up to 70–80 wt% occurred due to evolution of H_2O, CO_2,

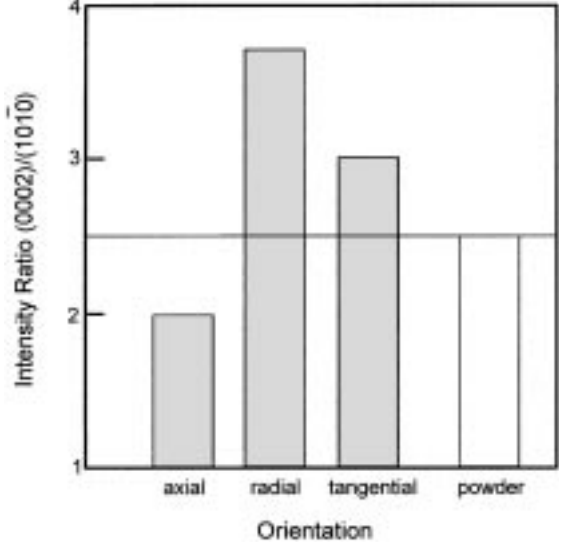

Fig. 6. XRD intensity ratios (0002)/(1010) of hexagonal carbon in the pyrolyzed carbon preform for different orientations.

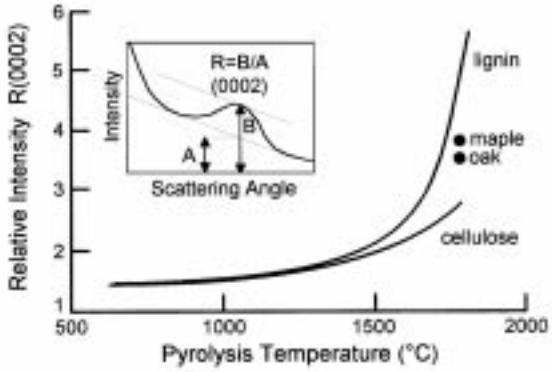

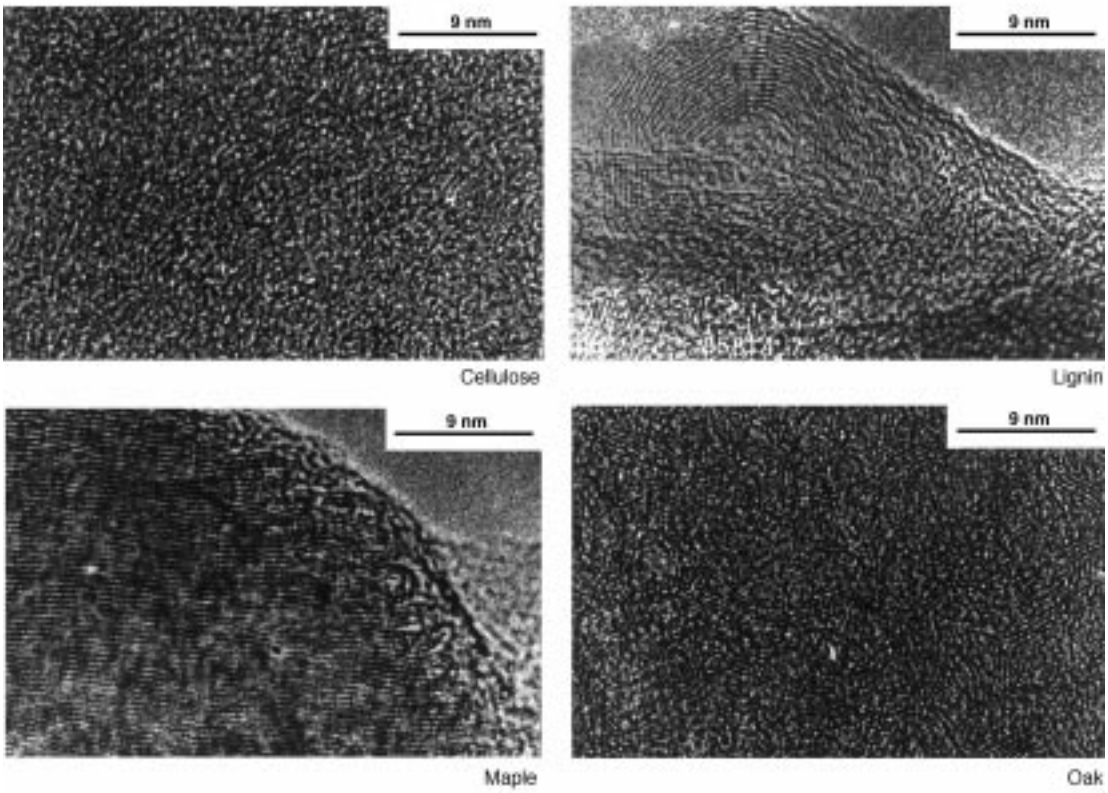

Fig. 5. Microstructural transformation of carbonized wood preform between 600–1800°C: (a) XRD-interisity ratio of $(0002)_c$: (b) high resolution, TEM micrographs after pyrolysis at 1800°C.

and volatile hydrocarbon species from fragmentation reactions of the polyaromatic constituents.[23] Figure 4 shows the basic products of thermal decomposition reactions of the major molecular constituents of natural wood. Different kinds of wood, however, may exhibit a wide range of weight loss due to the variation of molecular composition e.g. lignin to cellulose ratio and cellular structure. The aromatic structure of the lignin molecule which contains a high fraction of phenylpropane units combined through ether linkages or carbon-to-carbon linkages[24] gives rise to a weight loss of 55 wt% whereas cellulose, which is characterized by oxygen bonded glucose units, shows a significantly higher weight loss of 80 wt%. The weight loss data are given in Table 2. After break down of the –C–C– chains in the biopolymer structures aromatic polynuclear carbon structure starts to form at temperatures above 600°C.[25] Rearrangement of the polyaromatic carbon structures results in an

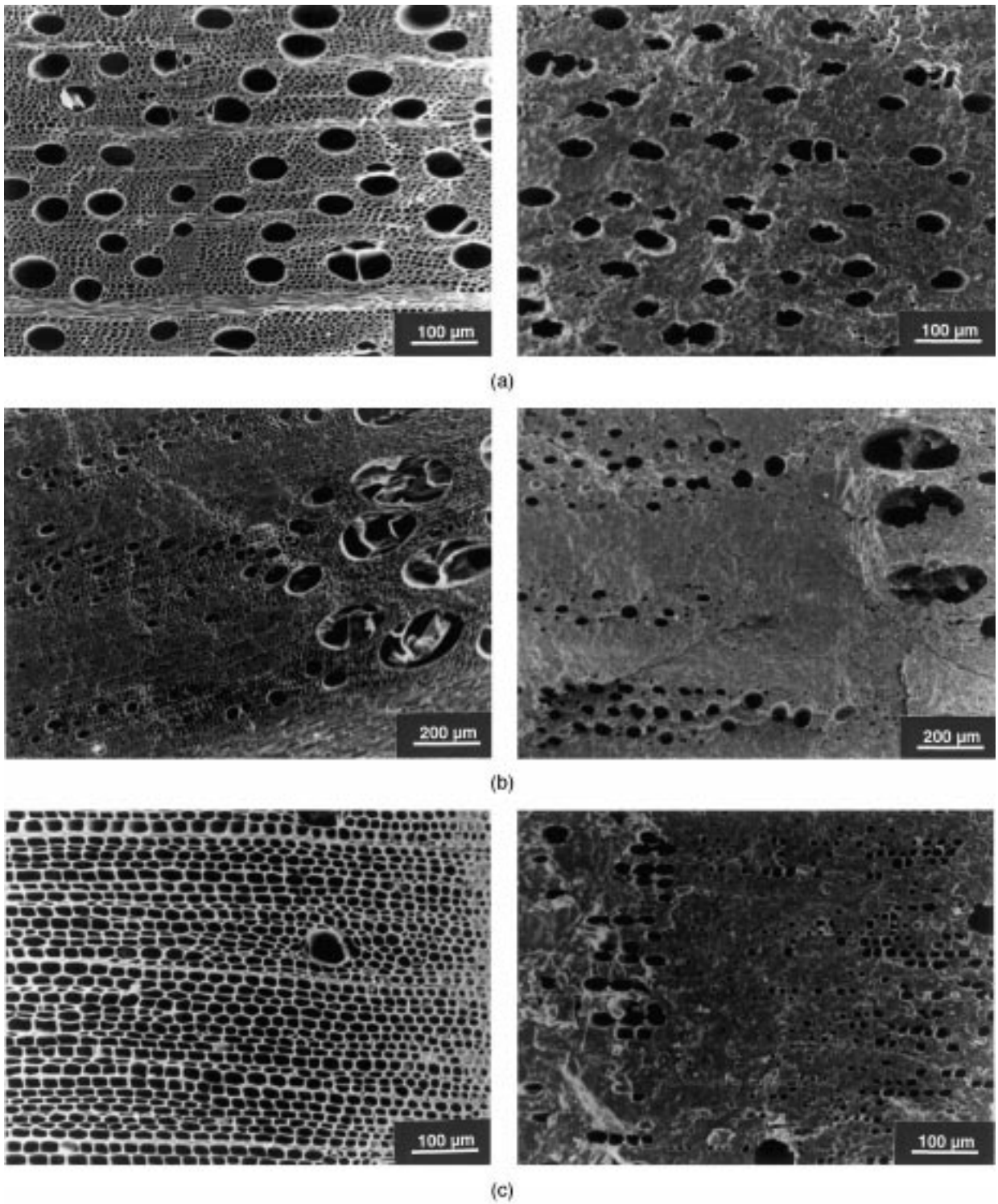

Fig. 7. Microstructures of carbonized wood preforms after pyrolysis at 1800°C (left) and after subsequent Si-infiltration and reaction at 1600°C (right): (a) maple, (b) oak, (c) pine, (d) beech and (e) balsa.

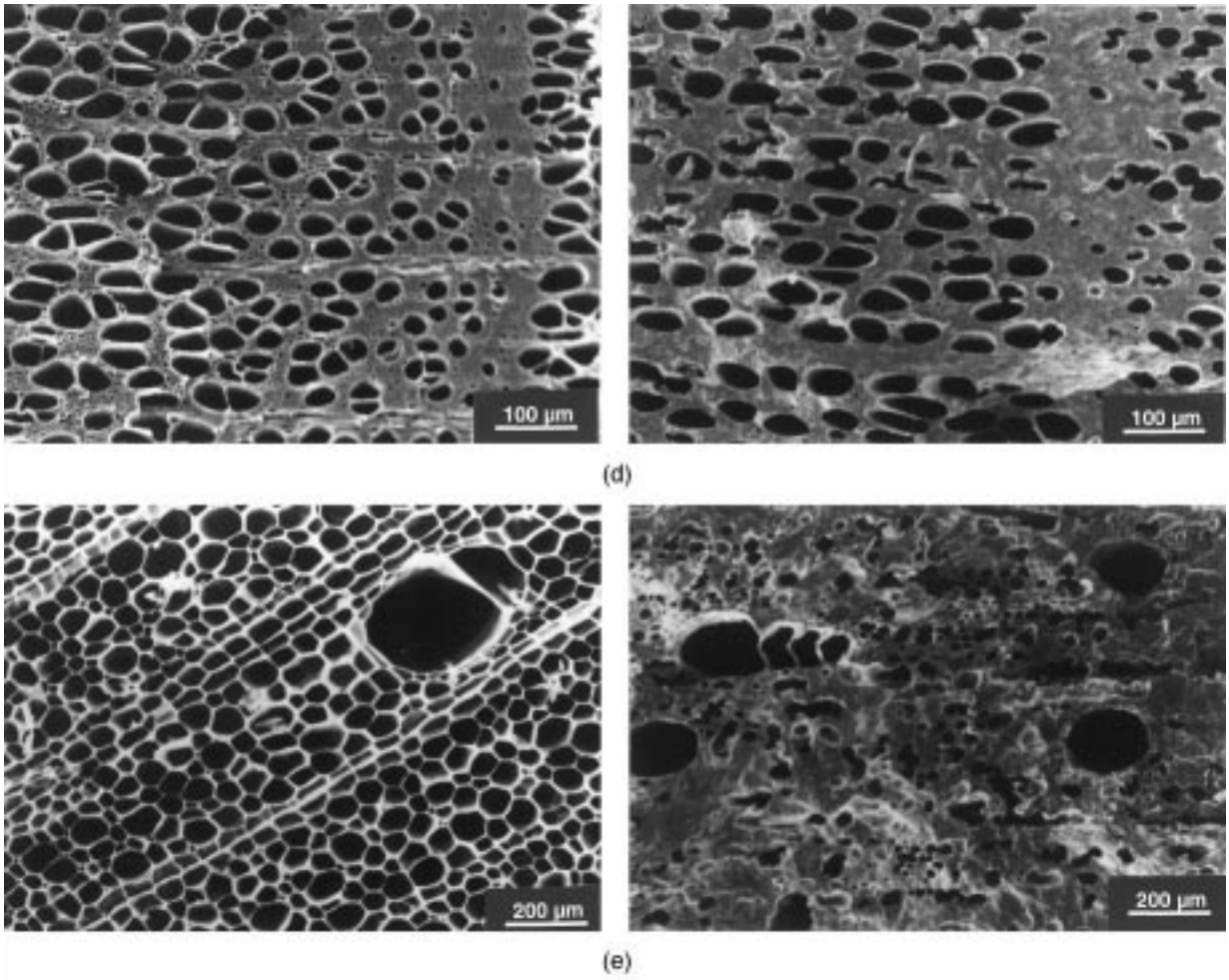

Fig. 7. *cont.*

increase of crystallinity as indicated by the increasing intensity and sharpness of the (0002) peak of hexagonal carbon at $d = 0{\cdot}3354$ nm (lattice constants of graphite are $a_0 = 0{\cdot}2461$ nm and $c_0 = 0{\cdot}6078$ nm). With increasing temperature as well as increasing lignin content of wood the degree of order of the graphitic like structural units increases significantly above 1400°C as indicated by XRD analysis of (0002) peak intensities and TEM analysis. Figure 5(a) shows the variation of (0002) peak intensity R (for definition of R see Fig. 5[26]) of pure cellulose and lignin in the temperature range from 600 to 1800°C compared with the data of maple and oak pyrolyzed at 1800°C. Lignin shows a significantly higher degree of order at 1800°C compared to cellulose whereas the natural wood samples which contain both biopolymers in various ratio exhibit an intermediate behavior as shown by the TEM micrographs given in Fig. 5(b). Analysis of peak intensities in different orientations reveal that the basic structural units of the hexagonal carbon exhibit a preferential orientation with respect to the dominating axial cell direction. Figure 6 shows the (0002)/(1010) intensity ratio of hexagonal carbon pyrolyzed oak in the axial, radial and tangential plane compared to a powder sample. Similar changes of intensity ratio were found for other corresponding directions as well. The reduced (0002)/(hki0) intensity ratios in axial orientation indicate that the basal plane (0001) of hexagonal carbon should be preferentially oriented parallel to the original tracheidal cell surfaces e.g. $[0001]_c$ perpendicular to the axial direction.

Pyrolysis of wood into the carbon preform involves an anisotropic shrinkage of approximately 20% in axial but 30% in radial and up to 40% in tangential directions, (Table 2). The magnitude of shrinkage anisotropy depends on the axial orientation of the cellulose fibers in the cell walls (macrofibrils) and the radially oriented ray parenchyma which provide a high stiffness of the cellular structure in axial and radial directions but allow a large strain in tangential direction during pyrolysis.[24] Total porosity of carbonized wood after pyrolysis is 20–25% higher than the initial density of (dried) wood. Despite the changes in porosity and anisotropic shrinkage the porous macro- and microstructure of the carbonized wood is retained after pyrolysis with high precision, (Fig. 7).

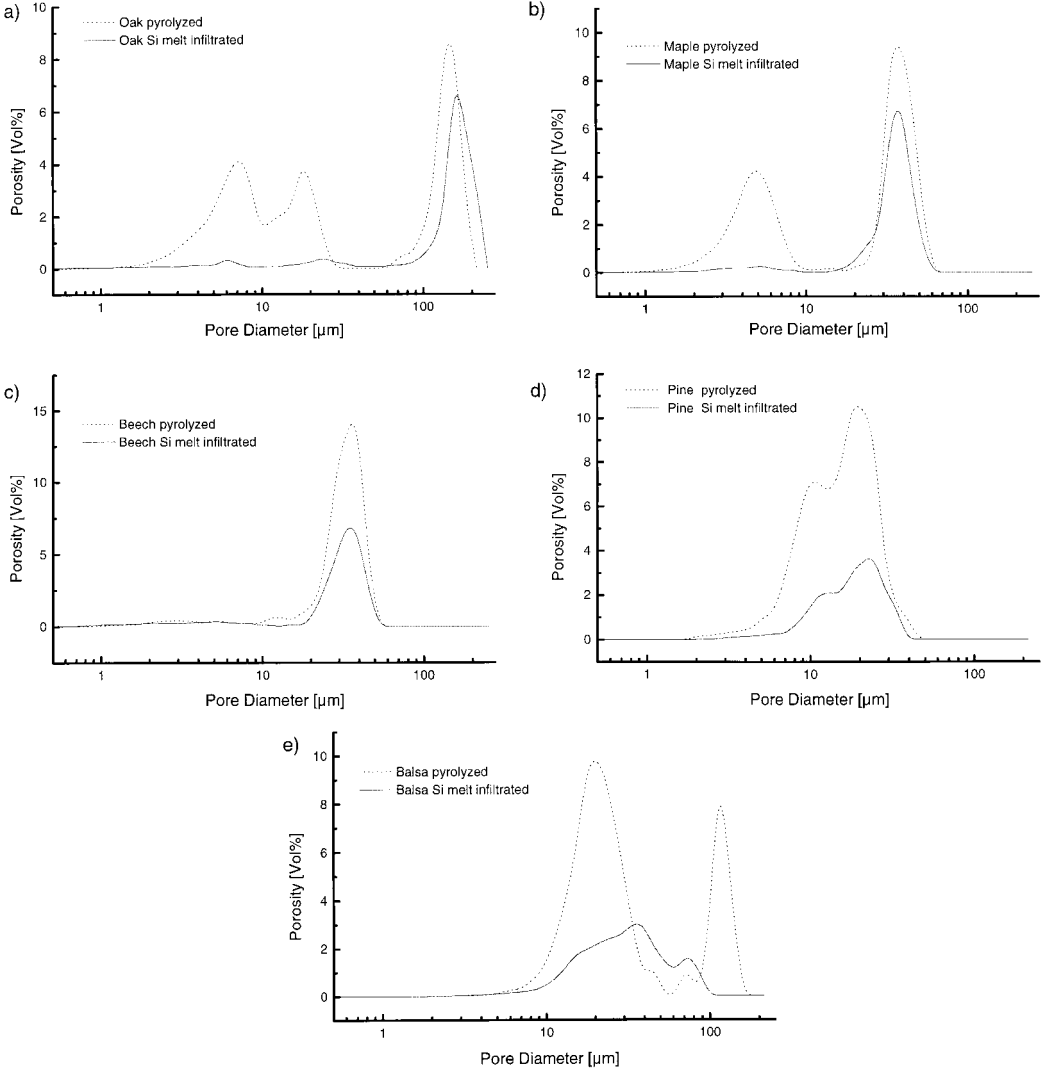

Fig. 8. Distribution of tracheidal cell diameters of wood after pyrolysis at 1800°C and after subsequent infiltration and reaction with Si at 1600°C.

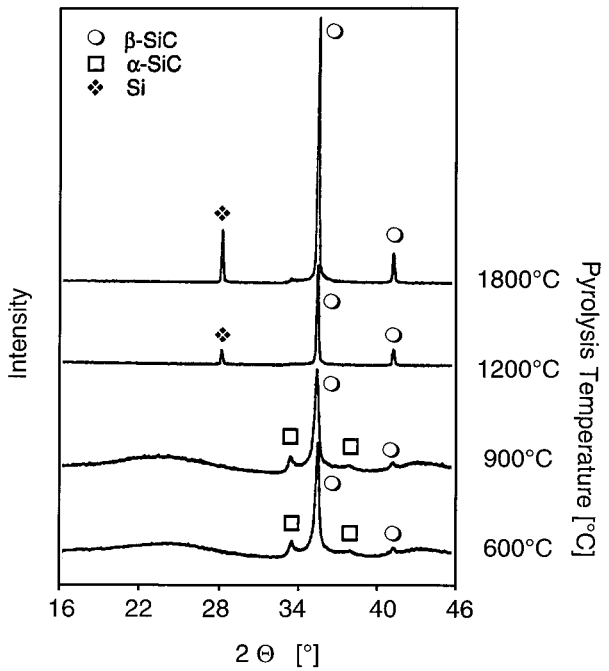

Fig. 9. XRD spectra of Si-infiltrated ceramic reaction products of oak.

3.2 Si-infiltration and reaction to SiC

Spontaneous wetting and infiltration of the porous carbon preform occurred when the tracheidal pore system was brought into contact with the silicon melt. Figure 8 shows the distributions of pore diameters in the carbon preform and after infiltration with silicon at 1600°C. Generally the carbonized preforms show a multimodal pore size distribution which is filled up with the silicon melt up to a maximum pore channel diameter of approximately 30 μm. Larger pores did not contain residual silicon, although the carbon template has completely transformed to β-SiC, (Fig. 9). In the case of carbonized balsa which has a porosity of >90% thermal shock may cause collapse of the carbon network when penetration of liquid silicon is too rapid.[27] The residual silicon content depends on the total porosity and the pore channel diameter distribution. As may be seen from Table 2 silicon content of the ceramic products pseudomorph to wood is between 23 wt% (maple) and 67 wt% (balsa) which is higher compared to

typical values of conventionally prepared SiSiC (20–30 wt%).[28]

Mean particle size of the β-SiC formed by reaction of penetrating silicon melt with the carbon in the pore channel surface is typically in the range of 5 μm. Figure 10 shows the EBSD patterns of β-SiC-crystals surrounding a tracheidal pore channel on an axial plane (residual silicon has been etched out of the pore channel). Analysis of orientation symmetry of the (001), (110) and 100) diffraction patterns suggests the β-SiC crystals are not randomly oriented but show a preferential orientationship. The possibility of oriented nucleation of β-SiC with respect to the microscopic and mezoscopic structure of the pyrolyzed cellular carbon structure will be discussed later.

4 Discussion

4.1 Reaction kinetics

When the porous carbonized preform comes into contact with liquid silicon spontaneous wetting may occur if the wetting angle $\Theta \ll 90°$. The wetting angle of Si depends on the surface structure of carbon: Θ was found to be less than 10° on (0001) planes of oriented polycrystalline pyrolytic graphite but 50° on vitreous carbon at 1450°C.[26] Hence molecular structure of pyrolyzed carbon on the pore surface is of particular importance for the infiltration behavior and generally is facilitated with increasing crystallinity of carbon. Spontaneous wetting forces the silicon melt to penetrate into the tracheidal pore channel system of the carbonized wood and concurrently the reaction to form β-SiC

$$\mathrm{C(s)} + \mathrm{Si(l)} \rightarrow \beta\text{-SiC}$$

takes place. The time required to achieve complete infiltration and reaction e.g. conversion of the carbonized preforms to the cellular ceramic product is limited by the infiltration and reaction kinetics which are a function of temperature. Wood structure in axial direction may be represented by a bundle of parallel capillaries (tracheidal cells) with the effective flow radius r which provide rapid access to the penetrating liquid silicon driven by capillarity. From the Poiseuille capillary flow equation

$$\frac{\mathrm{d}V}{\mathrm{d}t} = \frac{\pi r^3 \gamma \cos\Theta}{4\eta x} \tag{1}$$

time t to attain an infiltration depth x is given by[18]

$$t = x^2 \left[\frac{\gamma r\left(r^3/r_0^2 R\right)\cos\Theta}{2\eta}\right]^{-1} \tag{2}$$

The quantity in the nominator has the dimensions of a diffusion coefficient which depends on the effective capillary geometry and the properties of the infiltrating liquid e.g. surface tension γ, wetting angle Θ and viscosity η. Equation (2) takes into account that the effective capillary radius R (which drives the infiltration) may differ from r and the mean geometrical capillary radius $r_0 (r < R < r_0)$ due to irregularities in the voud spacings so that $(r^3/r_o^2 R) < 1$. Taking an infiltration depth x of 0.1 m as a reasonable order of magnitude and using literature data for the infiltration properties of liquid silicon at 1600° ($\gamma = 0{\cdot}82\ \mathrm{N\,m^{-1}}$ [30], $\Theta = 10°$[26], $\eta = 0{\cdot}7$ mPas[29]) a lower bound of the expected infiltration time can be derived. If $r = r_o = R$ it follows that t is in the range of 10–1 s for $r = 1 \ldots 10\ \mu$m which indicates that liquid silicon may readily be used for spontaneous infiltration of the carbonized wood preforms.

For the case of capillary wetting without applying an additional external pressure a maximum

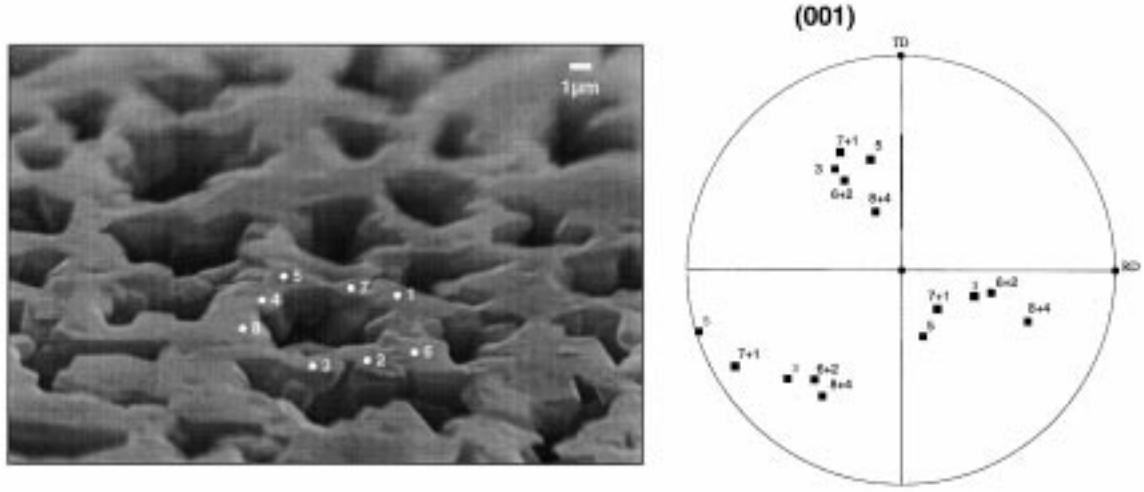

Fig. 10. EBSD patterns of β-SiC grains surrounding a tracheidal pore (Si was etched out).

capillary radius, R_{max} limits spontaneous infiltration perpendicular to the melt surface

$$R_{max} = \frac{2\gamma \cos \Theta}{\rho x} \tag{3}$$

For $x = 0.1$m an R_{max} of 60 and 40 μm is derived from eqn (3) for $\Theta = 10°$ and 50°, respectively. Pore size analysis before and after Si-infiltration shows that all pores with a diameter less than approximately 30 μm were completely filled up with Si whereas larger pores remained open, (Fig. 8).

Reaction of liquid silicon with carbon to form β-SiC simultaneously proceeds with infiltration as schematically indicated by Fig. 11. A detailed analysis of heterogeneous chemical reaction process for the combined effect of mass transfer from the liquid reactant (Si) to the solid (C) surface, the diffusion through the solid reaction product (β-SiC) and the chemical reaction between silicon and carbon revealed that after complete wetting is reached the reaction rate will be dominated by diffusion through the primary solid SiC-layer formed.[31] Assuming a diffusion controlled parabolic growth rate of SiC variation of reaction layer thickness d_{sic} over time can be expressed by

$$d_{sic} \approx \sqrt{D_{eff} t} \tag{4}$$

where the effective diffusion coefficient of through SiC is given as[31]

$$D_{eff} = D_0 \exp\left(\frac{-Q}{RT}\right) \tag{5}$$

Self-diffusion of silicon and carbon in silicon carbide has been measured for single-crystal and polycrystal samples. Both the carbon and silicon diffusivities have high activation energies and high pre-exponential terms, suggesting vacancy division mechanisms. With $D_0 = 2 \times 10^{-6}$ cm s^{-1} and an activation energy of $Q = 132$ kJ mol^{-1} a D_{eff} (1600°C) $= 4{\cdot}168 \times 10^{-10}$ cm^2 s^{-1} can be used to estimate the time of reaction to convert the carbonized cellular structure of wood with mean carbon layer thickness of 10 μm into SiC as 40 min. Figure 12 shows the variation of infiltration depth and reaction layer thickness with time for a range of pore radii and cell wall thicknesses. As may be seen, the ratio of infiltration depth to reaction layer thickness

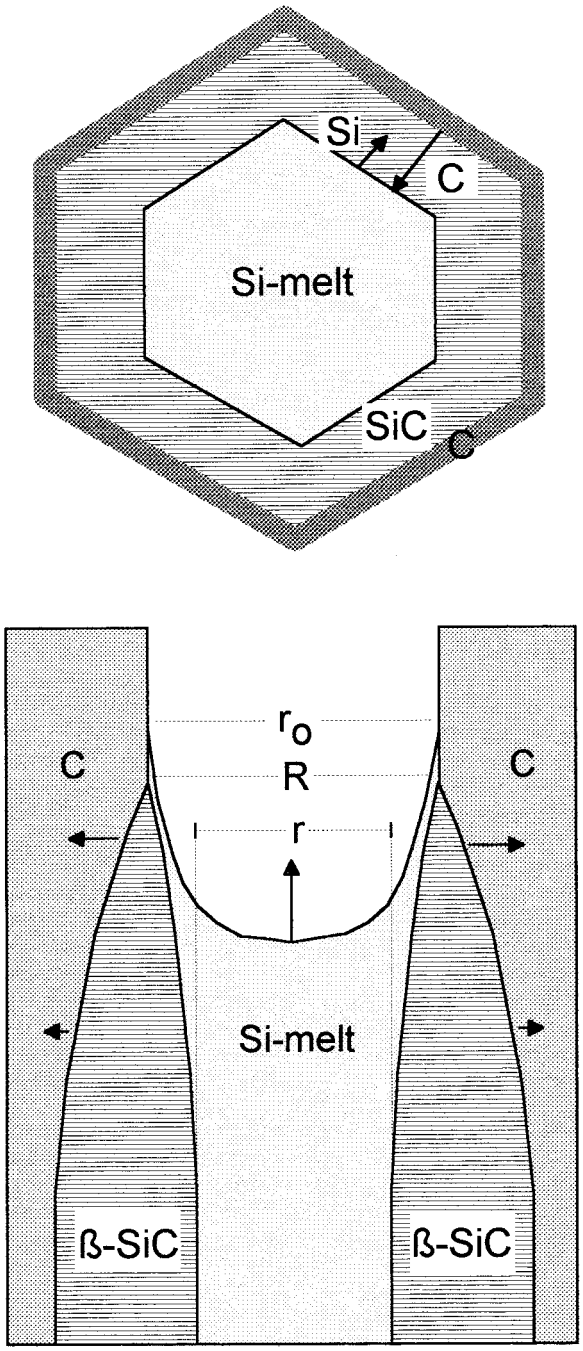

Fig. 11. Model of concurrent Si-melt infiltration and SiC-reaction process.

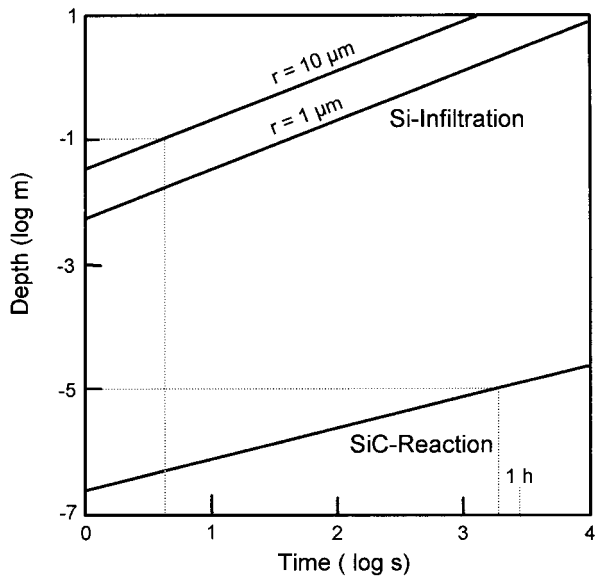

Fig. 12. Infiltration depth of liquid Si into the carbon preform and SiC-reaction layer thickness at 1600°C as a function of time.

is $1{\cdot}5\times10^5$ suggesting the SiC formation reaction to be the rate controlling factor in the overall carbon to ceramic conversion process.

4.2 Microstructural relationships

XRD analyses of texture generation in the carbon preform and EBSD analyses of β-SiC crystal orientation suggest that SiC nucleation may be influenced by the molecular structure and orientation of carbon in the pore surface. Reduction of $(0002)_c$ peak intensities in axial orientations indicates that the aromatic C_6-rings in the carbon layers of turbostratic carbon are aligned parallel to the original tracheidal cell surface with the $[0001]_c$-vector perpendicular to the axial direction, (Fig. 13). Wide angle X-ray spectroscopy and high-resolution SEM showed similar sheet like orientation of the basic structural units of polyaromatic carbon layers with the $[0001]_c$ direction perpendicular to the fiber elongation in carbon fibers derived from polyacrylnitril (PAN) and mesophase pitch-based carbon fibers.[32,33] It is suggested that the molecular orientation of the carbon induces a crystallographic texture of the β-SiC which after infiltration of liquid silicon nucleates at the pore surface. EBDS patterns, (Fig. 10), indicate that the β-SiC crystals are not randomly oriented but exhibit a specific orientationship with respect to the original carbon orientation. Figure 13 shows some of the possible lattice orientationships between the (0001) plane of carbon and the (110) plane of β-SiC which can form due to minimum lattice mismatch. Both $d_{(200)} = 0{\cdot}2174$ nm and $d_{(111)} = 0{\cdot}251$ nm of β-SiC exhibit only a lattice spacing difference of less than 2% between $d(1010) = 0{\cdot}2131$ nm and $2\times d_{(1120)} = 0{\cdot}2468$ of graphite ($a_0 = 0{\cdot}21461$ and $c_0 = 0{\cdot}6708$),

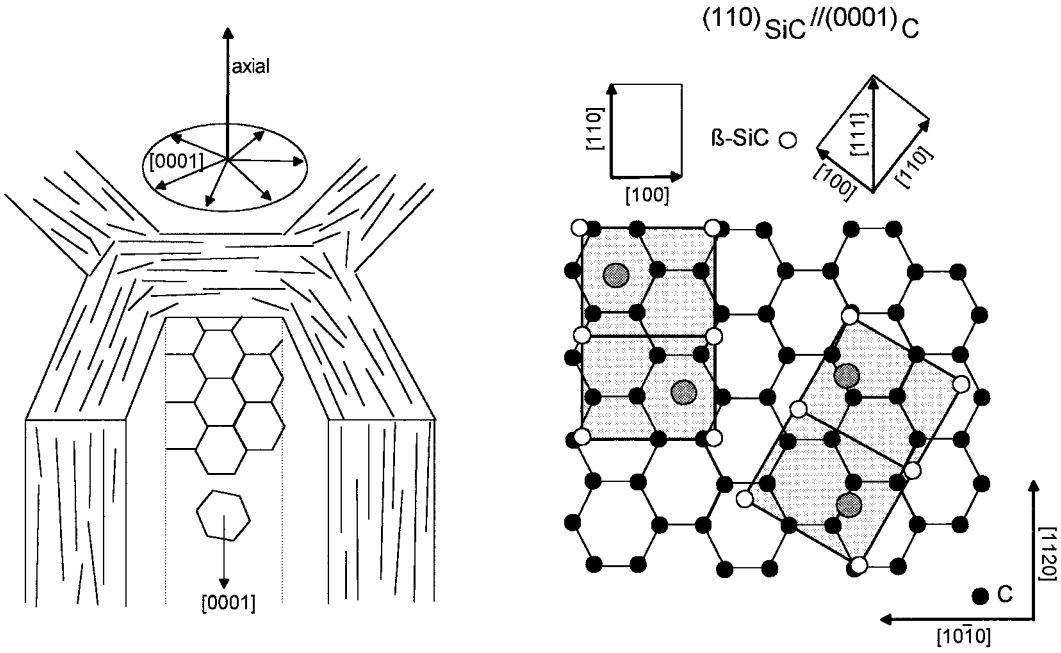

Fig. 13. Possible crystallographic textures of pyrolyzed carbon and Θ-SiC formed by liquid Si reaction with the carbon preform.

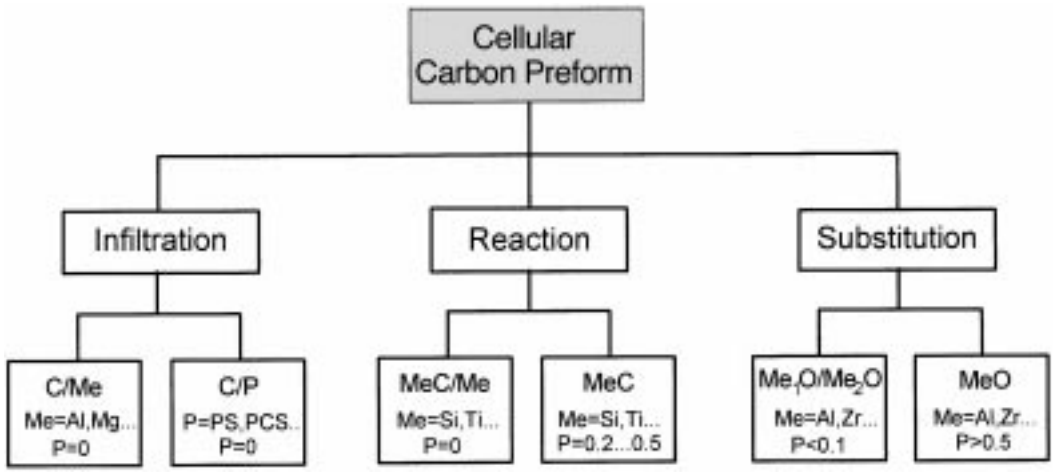

Fig. 14. Technology road map for manufacturing composite materials from pyrolyzed wood preforms (P: porosity).

respectively, which could facilitate an expitaxial nucleation with the $[110]_{sic}//[0001]_c$. The mechanical and elastical properties of such a cellular ceramic material will therefore not only be dependent on the meso- and macroscopic pore structure but will be additionally influenced by the crystallographic texture of the matrix material.

4.3 Other ceramics derived from the cellular carbon preform

The pyrolyzed porous carbon preform can be used for other synthesis reactions to form a variety of celullar ceramic composite materials, (Fig. 14). Infiltration of the porous carbon preform by non-reacting melts like Mg or Al (rapid infiltration under pressure avoids Al_4C_3 formation) or by low viscous polymers like conventional thermoplastics (PE, PVC, PA, etc,) or preceramic polymers (Polysilanes, -siloxanes, -carbosilanes, etc.) result in completely dense materials. Liquid infiltration with reacting melts like Si and Ti yield carbide/metal composites where the residual porosity is filled up with excessive metal. The reaction with gaseous infiltrants may yield single phase carbide ceramics with 20–50% open porosity. Infiltration with oxide forming sols/gels or suspensions and substitution of the carbon template by a second oxide forming infiltrant offers the possibility of producing celullar oxide ceramics of various composition.

5 Conclusions

Infiltration of the carbon preform derived from wood with liquid reactants such as Si or other metallic or non-metallic melts offers a versatile processing scheme to produce novel ceramics and ceramic composites with a unique oriented cellular microstructure. The anisotropy of their mechanical and other physical properties generally increases with porosity and great differences in strength, strain to failure, toughness, etc. may occur when loading is applied in axial, radial or tangential direction of the original wood structure. Anisotropic cellular ceramics of low density but high strength, however, could be of particular interest for applications in acoustic and heat insulation structures, as substrate, filter and catalyst carrier at high temperatures, as thermally and mechanically loaded ligth weight structures as well as for medical implant structures.

References

1. Aksay, I. A., Baer, E., Sarikaya, M. and Tirell D. A. (ed), Hierarchically structured materials. *Mat. Res. Soc. Symp. Proc*, Vol. 255. Mat. Res. Soc. Pittsburg/PE (1992).
2. Calvert, P., Biomimetic ceramic and composites. *Mat. Res. Soc. Bull.*, 1992, **17**, 36.
3. Sarikaya, M. and Aksay, I. A., An introduction to biomimeties: A structural viewpoint. In *Microstructure of Materials*, Krishnan, K. M. ed. San Francisco Press Inc., San Francisco/CA, 1993.
4. Mark, J. E. and Calvert, P. D., Biomimetic, hybrid and in situ composites. *Mat. Sci. Eng.*, 1994, **C1**, 159.
5. Mann, S. Webb, J. and Williarns, R. P. (ed). *Biomineralization—Chemical and Biochemical perspectives* VCH Weinheirn/Germany,1989.
6. Alper, M., The biological membrane. *Mat. Res. Bull*, 1992, **17**, 53.
7. Fink, D. J., Caplan, A. I. and Heuer, A. H., Eggshell mineralization: A case study of a bioprocessing strategy. *Mat. Res. Soc. Bull.*, 1992, **17**, 27.
8. Mann, S., Archibald, D. D., Didymus, J. M., Heywood, B. R., Meldrun, F. C. and Wade, V. J., Biomineralization: biomimetic potential at the inorganic–organic interface. *Mat. Res. Soc. Bull.*, 1992, **17**, 32.
9. Mann, S., Biomineralization, the inorganic–organic interface and crystal engineering, In Biomimetics—Design and Processing of Materials, AIP Press Woodburly/NY,1995 p. 91.
10. Patel, M. and Padhi, B. K., Production of alumina fibre through jute fibre substrate. *J. Mat. Sci.*, 1990, **25**, 1335.
11. Patel, M. and Padhi, B. K., Titania fibres through jute substrates. *J. Mat. Sci. Lett.*, 1993, **12**, 1234.
12. Krishnaro, R. V. and Mahajan, Y. R., Preparation of silicon carbide fibres from cotton fibre and silicon nitride. *J. Mat. Sci. Lett.*, 1996, **15**, 232.
13. Wagenführ, R., *Anatornie des Hoizes*. VEB Fachbucliveriag, Leipzig/GDR 2. Aufl. 1980.
14. Gibson, E. J., Wood: A natural fibre reinforced composite. *Metals and Materials*, 1992, **6**, 333.
15. Lucas, P. W., Darvell, B. W., Lee, P. K., Yuen, T. D. B. and Choong, M. F., The toughness of plant cell walls. *Phil. Trans. Roy. Soc. Lond.*, 1995, **B348**, 363.
16. Ota, T. Takahashi, M., Hibi, T., Ozawa, M. and Suzuki, H., Biomimetic process for producing SiC Wood. *J. Am. Ceram. Soc.*, 1995, **78**, 3409.
17. Greil, P., Lifka, T. and Kaindl, A., Biomorphic silicon carbide ceramics with cellular microstructure, to be publ. in *Proc. Ceramic Processing '97, September 1997* St. Barbara, CA, The American Ceramic Society, Westerville, 011 1998.
18. Hillig, W. B., Melt infiltration approach to ceramic matrix composites. *J. Am. Ceram. Soc.*, 1988, **71**, C96.
19. Chiang, Y. M., Messner, R. P., Terwilliger, C. D. and Behrendt, D. R., Reaction formed silicon carbide. *Mat. Sci. Eng.*, 1991, **A144**, 63.
20. Pampuch, R., Walasek. E. and Bialoskorski, J., Reaction mechanism in carbon–liquid silicon systems at elevated temperatures. *Ceram. Int.*, 1986, **12**, 99.
21. Dahn, J. R., Xing, W. and Gao, Y., The falling cards model for the structure of microporous carbons. *Carbon*, 1997, **36**, 825.
22. Ehrburger, P., Lahaye, L. and Wozniak, E., Effect of carbonization on the porosity of beechwood. *Carbon*, 1982, **20**, 433.
23. Byrne, F. F. and Marsh, H, Introductory overview. In *Porosity in Carbons*, Patrick, J. W. ed. E. Arnold Publisher, London, 1995.
24. Wenzel, H. F. J., *Chemical Technology of Wood*, Academic Press, London, 1970.
25. Shafizadeh, F. and Sekiguchi, Y., Development of aromaticity in cellulose Chars. *Carbon*, 1983, **21**, 511.
26. Whalen, T. J. and Anderson, A. T., Wetting of SiC, Si_3N_4, and Carbon by Si and Binary Si Alloys. *J. Am. Ceram. Soc.*, 1975, **58**, 396.
27. Ness, J. N. and Page, T. F., Microstructural evolution in reaction-bonded silicon carbide. *J. Mat. Sci.*, 1986, **21**, 1377.

28. Osada, H., Kanj, A., Katayama, S. and Koga, T., Bending strength and electrical resistivity of porous Si–SiC ceramics. *Ceram. Trans.,* Vol. 31, The American Ceramic Society, Westerville/OH 1993 243
29. Battezzati, L. and Greer, A. L., The viscosity of liquid metals and alloys. *Acta Metall.*, 1989, **37**, 1791.
30. Hardy, S. G., The surface tension of liquid silicon. *J. Crystal Growth*, 1984, **69**, 456.
31. Fitzer, E. and Gadow, R., Fiber-reinforced silicon-carbide. *Am. Ceram. Soc. Bull.*, 1986, **65**, 326.
32. Vezie, D. L. and Adams, W. W., High resolution scanning electron microscopy of PAN-based and pitch-based carbon fibre. *J. Mat. Sci. Lett.*, 1990, **9**, 883.
33. Kurnar, S., Anderson, D. P. and Crasto, A. S., Carbon fibre compressive strength and its dependence on structure and morphology. *J. Mat. Sci.*, 1993, **28**, 423.